DISCLAIMER

This report was prepared as an account of work sponsored by an agency of the United States Government. Neither the United States Government nor any agency thereof, nor any of their employees, makes any warranty, express or implied, or assumes any legal liability or responsibility for the accuracy, completeness, or usefulness of any information, apparatus, product, or process disclosed, or represents that its use would not infringe privately owned rights. Reference herein to any specific commercial product, process, or service by trade name, trademark, manufacturer, or otherwise does not necessarily constitute or imply its endorsement, recommendation, or favoring by the United States Government or any agency thereof. The views and opinions of authors expressed herein do not necessarily state or reflect those of the United States Government or any agency thereof. Reference herein to any social initiative (including but not limited to Diversity, Equity, and Inclusion (DEI); Community Benefits Plans (CBP); Justice 40; etc.) is made by the Author independent of any current requirement by the United States Government and does not constitute or imply endorsement, recommendation, or support by the United States Government or any agency thereof.

U.S.NRC
United States Nuclear Regulatory Commission
Protecting People and the Environment

Technical Letter Report

TLR-RES/DE/REB-2025-14

Computational Modeling of Graphite Degradation due to Molten Salt Infiltration and Wear

Date:

August 2025

Prepared in response to Task 4 in User Need Request NRR-2022-009, by:

Veerappan Prithivirajan
Idaho National Laboratory

NRC Project Manager:

Joseph Bass
Reactor Engineer
Reactor Engineering Branch

Division of Engineering
Office of Nuclear Regulatory Research
U.S. Nuclear Regulatory Commission
Washington, DC 20555–000

This report does not contain or imply legally binding requirements. Nor does this report establish or modify any regulatory guidance or positions of the U.S. Nuclear Regulatory Commission and is not binding on the Commission.

Page intentionally left blank

Computational Modeling of Graphite Degradation due to Molten Salt Infiltration and Wear

INL/RPT-25-86762

Nuclear Regulatory Commission

AUGUST 2025

Veerappan Prithivirajan

Idaho National Laboratory

Idaho National Laboratory

Battelle Energy Alliance manages INL for the U.S. Department of Energy's Office of Nuclear Energy

INL/RPT-25-86762

Computational Modeling of Graphite Degradation due to Molten Salt Infiltration and Wear

Veerappan Prithivirajan
Idaho National Laboratory

August 2025

Idaho National Laboratory
Computational Mechanics and Materials Department
Idaho Falls, Idaho 83415

http://www.inl.gov

Prepared for the
U.S. Department of Energy
Office of Nuclear Energy
Under DOE Idaho Operations Office
Contract DE-AC07-05ID14517

Page intentionally left blank

EXECUTIVE SUMMARY

Molten salt reactors (MSRs) are promising next-generation reactors, and in several such designs, graphite serves as the moderator and/or reflector. However, due to limited experimental data and operational experience, an understanding of the structural integrity of graphite in molten salt environments remains incomplete. This report presents a modeling-based evaluation of graphite degradation in MSR environments, focusing on the effects of salt infiltration in fuel-salt-based designs and surface wear in pebble-bed reactor designs. The objective of this study is to enhance the current understanding of the structural integrity challenges posed by these degradation mechanisms, and to provide a framework for assessing graphite behavior in MSRs.

The first part of this report investigates the phenomenon of molten salt infiltration into graphite. The infiltration occurs when molten salt permeates the interconnected pore structure of the graphite component, driven by factors such as pressure differentials and the physical properties of both the salt and graphite. The infiltration process is influenced by characteristics of the pore structure, the viscosity of the molten salt, and the interfacial energies between the graphite, salt, and the atmosphere within the graphite pore. By utilizing a coupled multiphysics modeling approach with the Grizzly software, the study evaluates the stress induced by internal heat sources from fission in the infiltrated salt, which can lead to structural concerns. This evaluation is crucial for understanding how infiltration affects the mechanical integrity of graphite components in MSRs. This study considers the Molten-Salt Reactor Experiment (MSRE) graphite moderator element geometry, due to relevant data on it being readily available.

Through detailed finite element analysis, the study examines stress distributions at varying infiltration percentages, revealing that stress levels increase with higher amounts of infiltration. Rare-event simulations, using the parallel subset simulation (PSS) framework, further quantify the failure probability under various input uncertainties, with a user-specified failure metric. The PSS framework also identifies input parameters that significantly affect the stress values, including infiltration amount, thermal conductivity, and power density. Additionally, considering realistic reactor scenarios, the analysis was performed to account for the combined effects of radiation and infiltration, and modeling strategies on how to analyze new MSR designs or new graphite grades are discussed.

The second part of this report focuses on wear mechanisms in pebble-bed-based MSRs. As graphite fuel pebbles interact with the graphite reflector block, wear can result in material loss and the formation of surface defects, which may act as stress concentrators. A similar multiphysics modeling framework, like the one used for infiltration, is employed to assess the impact of wear on the structural integrity of graphite components. This study considers a generic fluoride-cooled high-temperature reactor (gFHR) design, due to the availability of comprehensive data.

Worst-case scenario dimensions of the reflector blocks were analyzed under thermal and radiation conditions. Subsequently, wear in the form of idealized pits and grooves was modeled on the inner surface of the graphite block, using the maximum stress from previous simulations. The simulations show that groove-type defects are more detrimental than pits, leading to higher stress concentrations. Considering worst-case simulation scenarios and experimental wear rates, under the assumptions and inputs considered, it was determined that formation of a surface defect critical enough to affect the stress in a significant way is not possible in a gFHR design.

Overall, the findings of this research contribute to the development of robust modeling tools for predicting graphite behavior under various operational conditions in MSRs.

ACKNOWLEDGMENTS

The author thanks the following persons for their active participation in discussions, thoughtful questions, and valuable feedback—all of which significantly contributed to this report: U.S. Nuclear Regulatory Commission (NRC) staff Drs. Joseph Bass, Raj Iyengar, and Matthew Gordon, and Idaho National Laboratory (INL) colleagues Drs. William Windes and Benjamin Spencer. Additionally, the author is grateful to Drs. Mustafa K. Jaradat and Javier Ortensi from INL for providing neutron flux distributions and insightful discussions. The author also gratefully acknowledges his INL colleagues, Dr. Som Dhulipala for his assistance with parallel subset simulations and Dr. Daniel Schwen for his help in streamlining the workflow of infiltration simulations. The author also extends his special thanks to Drs. Nidia Gallego and Tomas Gretjak from Oak Ridge National Laboratory (ORNL) for their valuable inputs into the wear modeling study.

This manuscript was authored by Battelle Energy Alliance, LLC under contract no. DE-AC07-05ID14517 with the U.S. Department of Energy (DOE). The U.S. Government retains a nonexclusive, paid-up, irrevocable, worldwide license to publish or reproduce the published form of this manuscript, or allow others to do so, for U.S. Government purposes.

Page intentionally left blank

CONTENTS

FIGURES

TABLES

Page intentionally left blank

ACRONYMS

CTE	coefficient of thermal expansion
MCMC	Markov chain Monte Carlo
MOOSE	Multiphysics Object Oriented Simulation Environment
MSR	molten salt reactor
MSRE	Molten Salt Reactor Experiment
PSS	parallel subset simulation
TRISO	tri-structural isotropic

Page intentionally left blank

1. INTRODUCTION

Molten salt reactors (MSRs) represent an innovative reactor design that holds promise for the future of nuclear energy. However, they entail unique challenges due to the limited experimental data, operational experience, and analysis methods available for assessing their structural integrity. This report aims to address these challenges by employing modeling and simulation techniques to evaluate two critical degradation mechanisms: (1) molten salt infiltration into graphite in fuel-salt designs and (2) wear in pebble-bed-based MSRs.

1.1. Molten Salt Infiltration

The infiltration of molten salt into the interconnected pore structure of the graphite is driven by factors such as the pressure differential between the salt and the pore, pore characteristics, and the physical properties of the salt, including viscosity and the interfacial energies between the graphite, salt, and the atmosphere within the graphite pore. A higher pressure differential is required in order for the molten salt to infiltrate into smaller pores. Using ultra-fine and micro-fine grades of graphite can significantly reduce the amount of infiltration. However, infiltration of molten salt into graphite can have significant implications for the structural integrity of graphite components, particularly in fuel-salt-based reactor designs such as the Molten Salt Reactor Experiment (MSRE). Due to the fission process, infiltrated molten salt can act as a heat source, potentially compromising the structural integrity of the graphite. Given the limited experimental data available for such scenarios, modeling and simulation tools are essential for understanding the conditions under which structural integrity could be affected. A more detailed review of salt infiltration is provided in [4].

1.2. Wear in Pebble-Bed-Based MSRs

Wear in graphite components used in pebble-bed-based MSRs can occur due to abrasion and erosion mechanisms. In these reactors, graphite fuel pebbles rub against each other and against reactor structures, due to coolant circulation and pebble cycling, ultimately leading to material loss and surface defects. The severity of the wear is influenced by factors such as temperature, environment, and the presence of lubricants. For instance, tribological studies have shown that wear and friction are more pronounced at lower temperatures and in dry conditions, whereas higher-temperature environments with molten salt significantly reduce friction and wear rates. There is a concern that surface defects introduced by wear can act as stress concentrators, potentially leading to structural failure. In the present study, worst-case scenarios were simulated to evaluate the structural integrity of graphite components in pebble-bed-based MSRs. A more detailed review of graphite wear in MSRs is provided in [4].

1.3. Report Organization

This report discusses modeling and simulation tools for assessing new MSR designs and different graphite grades, offering general conclusions based on simulations of specific designs and graphite grades. The report is organized as follows. Section 2 discusses the role of molten salt infiltration, including the phenomena, their potential effects, and the modeling framework used to evaluate the stress induced by infiltration. Section 3 focuses on the role of wear in pebble-bed-based MSRs, including the phenomena, potential effects, and modeling framework used to evaluate structural integrity in the presence of wear. Section 4 summarizes the key findings of this study.

2. ROLE OF MOLTEN SALT INFILTRATION

2.1. Phenomena and Potential Effects

Molten salt infiltration into graphite occurs when the salt physically permeates the interconnected pore structure of the graphite. Molten salts generally are non-wetting fluids (i.e., the contact angle of the molten salt on graphite exceeds 90°). Therefore, for infiltration, a net positive pressure differential is required in order for the molten salt to be driven into the graphite pores. Apart from the pressure differential, various other factors influence the process of infiltration, including the pore characteristics and the physical properties of the salt (e.g., contact angle, surface tension, and viscosity). The minimum pressure differential (ΔP) required for infiltration is given by the Young-Laplace equation:

$$\Delta P = -\frac{4\gamma \cos\theta}{d}, \tag{1}$$

where γ is the surface tension of the molten salt, θ is the contact angle between the molten salt and the graphite surface, and d is the pore diameter. Readers can refer to [4] for a more detailed explanation.

In scenarios involving a fuel-salt-based reactor design such as the MSRE, the infiltration salt can act as a heat source as a result of the fission process, potentially impacting the graphite's structural integrity. Due to limited experimental data pertaining to such scenarios, we relied on modeling and simulation tools to understand the conditions under which structural integrity could be compromised.

2.2. Modeling Framework

This study primarily investigated the stress induced due to the internal heat source from molten salt infiltration, using a coupled multiphysics approach. A coupled thermo-mechanical model was employed to calculate displacements, temperature fields, strains, and stresses within a finite element framework. A steady-state heat transfer model, incorporating both conduction and convection, was used to determine the temperature fields. These temperature distributions were then applied to solve for stresses by using Cauchy's equation—specifically, the stress-free divergence equation. The simulations were conducted within the Multiphysics Object Oriented Simulation Environment (MOOSE) framework, which effectively handles complex multiphysics interactions.

An additive formulation for the total strain was employed, given by:

$$\epsilon^{total} = \epsilon^{elastic} + \epsilon^{thermal}, \tag{2}$$

where ϵ^{total}, $\epsilon^{elastic}$, and $\epsilon^{thermal}$ are the total strain, elastic strain, and thermal strain, respectively. $\epsilon^{thermal}$ is given by:

$$\epsilon^{thermal} = \alpha \Delta T. \tag{3}$$

Graphite components in a nuclear reactor are subjected to temperature gradients and boundary constraints, and stresses are expected to be induced. In graphite-moderated fuel-salt based MSRs, there is an additional component of volumetric heating with infiltration. If radiation effects are to be included, additional terms in strain have to be incorporated (e.g., the strain due to irradiation-induced dimensional change and irradiation creep) [5]. Furthermore, material property changes due to radiation must also be considered.

Key inputs to the thermomechanical simulation include the geometry of the graphite component, its thermomechanical properties, the reactor power density, and the appropriate boundary conditions. This work also presents a parallel subset simulation framework for obtaining the failure probability and the distributions of input parameters corresponding to a user-defined failure metric. Here, failure refers to a simplified allowable stress metric that solely assesses structural integrity. This metric does not account for functionality or safety functions.

2.2.1. Geometry and Properties

For finite element simulations of thermomechanical problems, multiple input data (e.g., geometry, temperature distributions, and power density) are critical. Given the necessity of these data, we chose the MSRE graphite moderator as our test problem, as it is one of the few reactors for which data are publicly available [6]. For reactors currently under development, much of the necessary data are inaccessible in the public domain. Additionally, nuclear graphite grade IG-110[a] was selected for the study, due to the availability of thermomechanical property data. While this choice was primarily data-driven, it also enabled this analysis to obtain critical insights and allowed for the development of a generalized modeling workflow adaptable to different component designs or graphite grades, based on provided inputs.

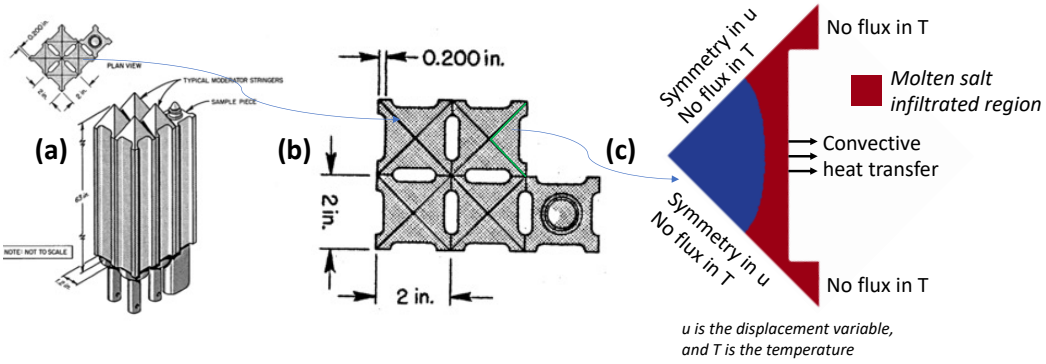

Figure 1. Schematic of the graphite moderator assembly in the MSRE: (a) full assembly, (b) cross section showing the graphite moderator and salt/coolant channels, and (c) unit cell of the moderator, with finite element simulation boundary conditions.

Table 1. Material properties of unirradiated graphite used in simulations [3].

Property	Unit	Value
Young's modulus	GPa	9.8
Poisson's ratio	-	0.14
Thermal conductivity	W/mK	63
Specific heat	J/kg	1400
Density	kg/m³	1760
CTE	/K	4.50×10^{-6}

[a]Note that IG-110 was not used in the MSRE. Instead, another nuclear graphite grade called CGB was used. CGB is highly anisotropic and is not currently being considered for any known reactor designs.

2.2.2. Finite Element Model

The actual moderator geometry, depicted in Figure 1(a), consists of a complex assembly of multiple graphite moderator elements. Each element is machined from CGB graphite, measuring 63 inches in height and 1.2 inches in width, and contains a total of 1,140 coolant passages [6]. A cross section showing the arrangement and coolant channels is given in Figure 1(b). Furthermore, to simplify the simulation setup, a quarter-symmetry model of a graphite moderator element with symmetric boundary conditions was used, as shown in Figure 1. This approach significantly reduces the computational cost yet maintains accuracy. The full assembly (Figure 1[a]) illustrates the overall configuration of the MSRE graphite moderator, while the cross section (Figure 1[b]) highlights the arrangement of the moderator and coolant channels. A unit cell of the moderator (Figure 1[c]) was used for the finite element simulation. Symmetric boundary conditions were applied to represent the larger system, ensuring efficient computation while capturing the essential physics of molten salt infiltration and its effects on the graphite component.

The boundary conditions prescribed in the 3D finite element model are shown in Figure 1(c). Symmetry boundary conditions in displacement as well as heat flux were enforced on the surfaces of the unit cell, as shown in Figure 1(c). Convective heat transfer was prescribed on the coolant channel boundary. The bottom surface of the unit cell was constrained in the out-of-plane displacement direction. Lastly, the effect of salt infiltration was accounted for as a volumetric heat source (refer to the red patch in Figure 1[c]). The fuel salt temperature along the length of the moderator element, as well as the fuel salt power density for the MSRE design, are provided in Figure 2 [7].

We also conducted 2D simulations, which will be discussed later. In these cases, a single 2D slice of the graphite moderator element was used as the geometry input for the simulations. All the boundary conditions, including the convective heat transfer, were the same as in the 3D model, but instead of applying them on a surface, they were applied on a line or curve. The interface temperature and power density values were taken as a single value at the center of the moderator element, where the power density is at its maximum.

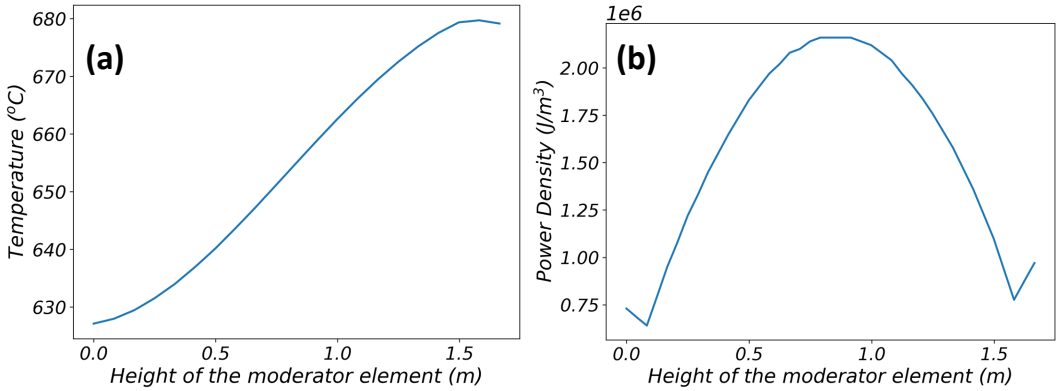

Figure 2. (a) Variation in salt temperature and (b) distribution of power density from the fission process, along the graphite moderator's length.

The extent of molten salt infiltration is influenced by many different factors, as discussed in Section 2. However, in this study, we adopted an inverse modeling approach; we did not attempt to determine the actual extent of the infiltration. Instead, we assumed the infiltration had occurred, and analyzed the resulting stress for varying levels of infiltration. This approach enabled us to identify conditions under which infiltration-induced stress could compromise the structural integrity of the graphite component.

Given the geometry, initializing the infiltration profile was not straightforward. To address this, we

employed a diffusion equation—similar to porous flow models—to establish a physically realistic infiltration profile before proceeding with the stress analysis. The boundary conditions were as follows: no flux at the left and bottom surfaces, and a concentration of unity was specified at the coolant channel boundary present on the inclined surface. The infiltration profile was obtained based on a user-defined infiltration percentage. While this approach is valid for both 2D and 3D simulations, we present the 2D results. Figure 3 illustrates these results, showing three different profiles corresponding to 25%, 50%, and 75% infiltration[b], with the red regions indicating molten salt and the blue regions representing the unaffected graphite. The infiltration profiles are curved as shown, which is as expected since symmetric boundary conditions were prescribed. The serrations near the boundaries are a result of the mesh structure, which do not impact the stress analysis. Additionally, while performing the stress analysis, the heat source was assumed to originate from fission of the molten fuel salt, and thus will occur in the red regions.

Accurately representing the pore structures within the graphite component presents additional challenges. The fact that the length scale of the pore is at least two orders of magnitude smaller than the component itself makes resolving these details in a finite element mesh impractical. Additionally, capturing an accurate pore distribution requires sophisticated imaging techniques not feasible at the component scale. To simplify the modeling approach, we assumed the molten salt to be distributed throughout the entire region defined by the infiltration profile. However, the internal heat source due to infiltration was scaled by the porosity fraction, ensuring that the total heat generation remained consistent but was applied in a distributed manner.

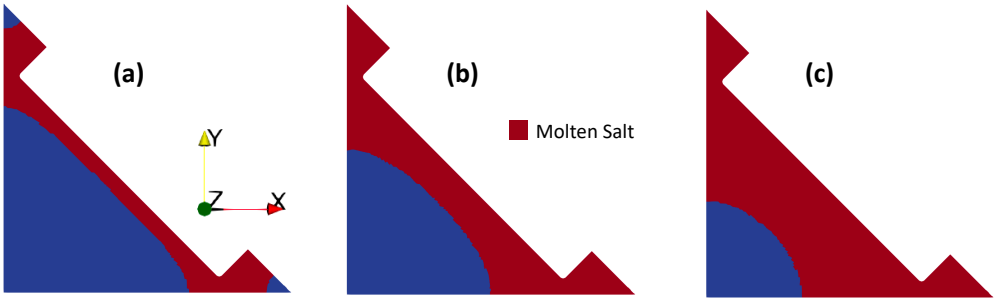

Figure 3. Profiles obtained from diffusion equation-based simulations for varying percentages of infiltration into the unit cell of the graphite moderator: (a) 25%, (b) 50%, and (c) 75%. In the figure, red-colored regions represent the molten salt infiltrated graphite, and blue represents the unaffected region.

2.2.3. Parallel Subset Simulations

Parallel subset simulation (PSS) is a stochastic sampling method designed to efficiently estimate failure probabilities for rare events[c], particularly in scenarios in which direct Monte Carlo methods would be computationally prohibitive. Instead of relying on an enormous number of samples to capture rare failure events, PSS breaks down the overall failure probability into a series of intermediate steps by defining a sequence of failure thresholds, as shown in Figure 4. At each step, the method conditions on the event that the output exceeds a certain threshold, effectively narrowing the sampling space toward the rare-event region. Markov chain Monte Carlo (MCMC) techniques are then used to generate samples that satisfy these conditional criteria, ensuring targeted and efficient exploration of the failure domain.

[b]75% infiltration means that 75% of the open pores have been filled by the molten salt. This assumes that the pressure differential is sufficient to fill the smaller pores, which is a conservative assumption.

[c]In the context of failures, a rare event typically refers to an occurrence that happens infrequently or has a very low probability of happening. These events are often unexpected and can have significant consequences.

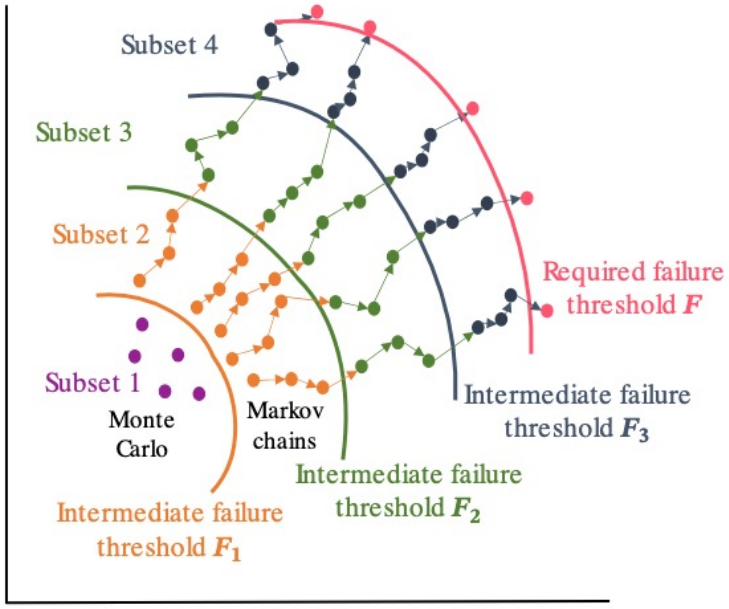

Figure 4. Schematic of the PSS method, illustrating subsets with internally parellelized evaluations advancing through progressively refined thresholds for efficient rare-event probability estimation (reproduced with permission from [1]).

Within the MOOSE framework, PSS is implemented such that the power of parallel computing is harnessed. Multiple independent Markov chains run concurrently on separate processors, significantly reducing the computational time required for convergence. Users can specify parameters such as the number of samples per subset, the total number of subsets, and the conditional probability that defines each intermediate failure threshold. This modular and parallel approach not only enhances the efficiency of the simulation but also integrates seamlessly with MOOSE's uncertainty quantification tools, enabling robust risk assessment and design optimization for complex multiphysics problems.

In this study, PSS was employed to identify the distribution of input parameters that could lead to failure based on predefined metrics. It also helps in understanding the significance and sensitivity of each input parameter concerning the failure criteria. This framework is invaluable for pinpointing critical factors behind potential failures, thus facilitating more informed and risk-aware decision making.

2.3. Simulation Results

In this section, we present the different simulation cases for the graphite moderator element, along with the corresponding results and analysis.

2.3.1. 3D Simulations

Initial simulations were conducted on the 3D unit cell geometries for varying levels of infiltration—namely, 0%, 33%, 67%, and 100%—to assess the stress induced, with the material properties and other inputs kept constant. As graphite is a quasi-brittle material, maximum principal stress would be an appropriate stress measure to analyze, as it is an indicator of failure. To that end, the maximum principal stresses obtained for

various infiltration amounts are shown in the Figure 5. The first case is the baseline case with no infiltration; the other cases reflect progressively increasing infiltration in the amounts mentioned above. For the baseline case, the maximum stress was approximately 0.0055 MPa at the boxed location, as shown in Figure 5(a). This coincides with the inflection point of the temperature profile at an axial coordinate of $\sim$1.5 m (Figure 2[a]). As infiltration increased, the location of maximum stress shifted toward the center of the moderator element, aligning with the power density profile (Figure 2[b]). At infiltration levels of 33%, 67%, and 100%, the maximum stresses were near the center of the moderator element. The magnitudes of these stresses were approximately 0.013 MPa, 0.04 MPa, and 0.13 MPa, respectively. Therefore, the highest infiltration levels induced higher stress, though the stress values were too small to cause any structural integrity issues. This setup was a coupled thermo-mechanical system, and the stresses induced are due to the temperature gradients and constraints in the system. To draw further insights into the location of the maximum stress, the steady-state temperature distributions at the respective cut sections passing through the maximum stress location for 33% and 100% were analyzed with their respective maximum stress distributions, as shown in Figure 6. It was observed that both cases had distinct temperature distributions and resulting stress distributions. The maximum tensile stress locations (which are circled in Figure 6) corresponded to cooler regions of the domain, which was as expected since hotter regions undergo thermal expansion whereas cooler regions experience tensile stress to maintain compatibility.

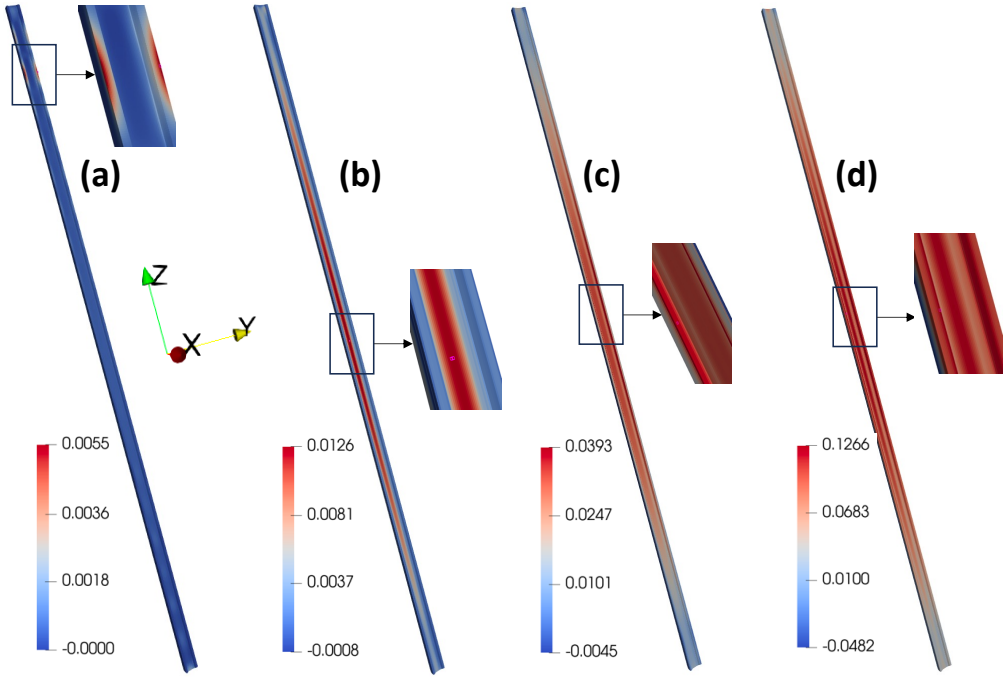

Figure 5. Maximum principal stress (MPa) variation induced by volumetric heating due to salt infiltration at different levels: (a) 0%, (b) 33%, (c) 67%, and (d) 100%.

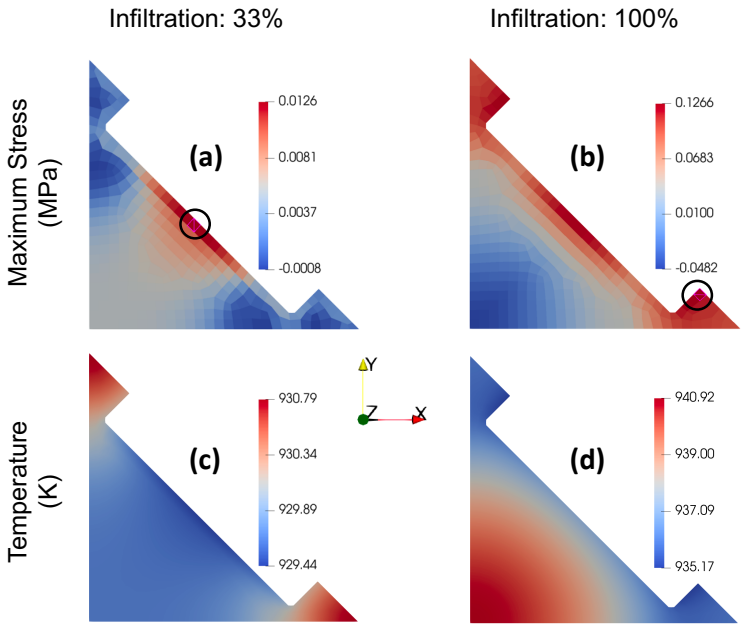

Figure 6. Comparison of maximum principal stress and temperature distributions at the cross section of the maximum stress location for (a) 33% and (b) 100%.

2.3.2. Reduced Model

The simulations mentioned above were conducted using a fixed set of material properties and previously discussed MSRE data. To understand the impact of molten salt infiltration on stresses, it is necessary to examine how stress changes with input parameters. This is crucial for evaluating graphite components in a new MSR design, or a new grade of graphite. Identifying the most sensitive parameters and obtaining the input distribution for a given failure metric is essential. Since this requires numerous simulations, we first assessed a simplified 2D generalized plane strain model for accuracy.

The maximum principal stress obtained from the full 3D model at the slice corresponding to the maximum stress location was compared to the results garnered from the 2D generalized plane strain setup, as shown in Figures 7(a) and (b), respectively. In addition, the absolute difference in the stress fields between the two simulation approaches is illustrated in Figure 7(c). It is evident that the generalized plane strain model accurately captures the maximum stress distribution, with an absolute error of less than 4%[d]. Thus, the parametric analysis was conducted using the 2D generalized plane strain setup in order to obtain insights while also significantly speeding up the computations.

[d]The 2D generalized plane strain model's accuracy, with an error in maximum stress of less than 4%, is acceptable for this study. The 2D model is suitable for extensive parametric analyses, providing reliable insights while speeding up computations. The PSS framework is also applicable for the full 3D model, which designers can use for more detailed analyses if needed.

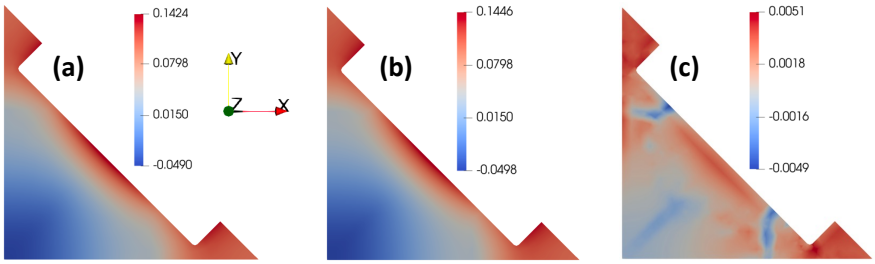

Figure 7. Comparison of maximum principal stress (MPa) distributions from (a) a full 3D simulation and (b) a 2D generalized plane strain approximation; (c) absolute difference in the stress fields, as obtained from (a) and (b).

2.3.3. Rare-Event Simulations

Eight input parameters were selected to analyze their impact on the maximum principal stress. For these studies, a 2D section of the MSRE moderator element geometry was utilized. The input parameters, particularly the power density and interface temperatures, were represented by single values corresponding to the center section of the 3D moderator element geometry. The input parameters were assumed to follow a uniform distribution, and the range of values used in the simulations are shown in Table 2. For these sets of simulations, the failure metric was chosen be to a maximum principal stress exceeding 15 MPa[e]. A total of 7,000 simulations were conducted, divided into seven subsets comprised of 1,000 simulations each. The first 1,000 simulations were conventional Monte-Carlo simulations, and the rest were designed to gradually move toward the failure point, by the PSS framework. This is evidenced by Figure 8, which shows the change in the component's maximum stress with changing subset samples. The mean value of the maximum stress is gradually increasing from the first subset (2.5 MPa) to the final subset (15 MPa), with many simulation cases exceeding the failure criteria. Furthermore, using the PSS framework, the failure probability was calculated to be 6.79E-7[f]. This implies that, considering all variations in the input parameters (which could potentially be related to reactor conditions), the probability that the MSRE graphite moderator element geometry with the stated assumptions would exceed a maximum principal stress of 15 MPa is approximately 1 in 1.5 million.

The output data from the simulations were analyzed using a Python script, which extracted the distributions of the input parameters corresponding to failure events. These distributions were then plotted alongside the Monte Carlo samples that pertained to the first subset, so as to derive critical insights. Figure 9 illustrates these comparisons for six input parameters: infiltration amount, Young's modulus, thermal conductivity, Poisson's ratio, and the coefficient of thermal expansion (CTE). In the figure, the Monte Carlo samples, depicted as blue histograms, represent the actual distribution of the inputs, whereas the failed samples, shown as red histograms, represent the distribution of inputs that contributed to the component's failure, based on the predefined criteria.

[e]The value of 15 MPa was chosen based on the maximum allowable tensile stress for IG-110, assuming a two-parameter Weibull distribution with a probability of 1e-4 [8]. A designer may also opt for more sophisticated criteria such as the American Society of Mechanical Engineers (ASME) full assessment. However, the major conclusions of this work, including the trends of inputs affecting the stress, will not change based on the choice of failure metric.

[f]The failure probability was estimated using the final subset in the PSS sequence (Figure 8). Out of the 1,000 samples in the last subset, 679 were found to exceed the failure threshold of 15 MPa. Given that each intermediate level in the PSS method was constructed to retain the top 10% of samples (i.e., a conditional probability of 0.1), and that the final subset corresponds to the seventh level, the total failure probability was computed as:

$$P_f = 0.1^6 \times \frac{679}{1000} = 6.79 \times 10^{-7}.$$

The exact number of subsets is not critical, provided the final subset is chosen such that some of the PSS output exceeds the failure metric. As shown in Figure 8, either subset 6 or subset 7 can be chosen as the final subset for failure probability calculations.

Table 2. Input parameters considered for rare-event simulations, along with their respective ranges.

No.	Parameter	Unit	Min	Max
1	Infiltration Depth	%	0	100
2	Young's Modulus	GPa	10	15
3	Thermal Conductivity	W/mK	25	105
4	Power Density	MW/m^3	10	250
5	Poisson's Ratio	-	0.13	0.21
6	Interface Temperature	K	923	1123
7	Heat Transfer Coefficient	W/m^2K	3500	5500
8	CTE	/K	3.50×10^{-6}	6.00×10^{-6}

Significant differences between the failure distribution and the Monte Carlo distribution indicate the factor under consideration to be critical. For instance, the figure reveals substantial effects stemming from infiltration amount, Young's modulus, thermal conductivity, power density, and CTE. Specifically, failure tends to occur with very high infiltration amounts, high Young's modulus values, very low thermal conductivity values, and high values of power density and CTE. Conversely, the distributions of insignificant parameters in the failed samples closely resemble those of the Monte Carlo samples. This pattern was observed for Poisson's ratio, interface temperature, and heat transfer coefficient. Consequently, only the plot for Poisson's ratio is included in Figure 9. It should be emphasized that failure can only occur if all input parameters fall within the corresponding failed sample distributions. If any parameter does not meet this criterion, failure will not occur.

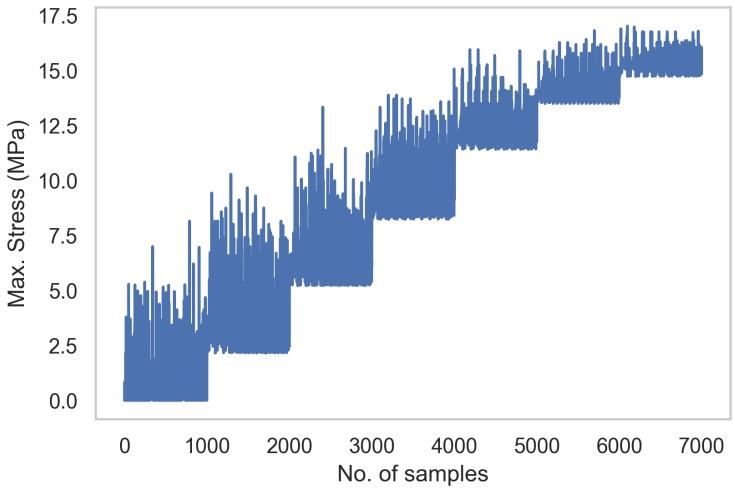

Figure 8. Evolution of maximum stress when using the PSS method. The stepwise pattern illustrates a consistent increase in average maximum stress across subsets as the PSS progresses, indicating a systematic shift of the input parameter space toward higher stress levels and potential failure.

The previous set of simulations was performed on the 2D section of the MSRE moderator element geometry, which does not provide insights into the effects of changing the geometry. To address this, a new moderator element geometry was created by uniformly scaling all dimensions of the 2D section of the original MSRE geometry by 150%. The rare-event simulations were repeated for this new geometry, using the same set of inputs and maintaining the same range of values. The failure probability for this setup was found to be 3.81E-3 ($\sim$1 in 262), which represents a significant increase as compared to the baseline MSRE moderator. Figure 10 illustrates the results of these simulations. From these results, it can be inferred that the failure

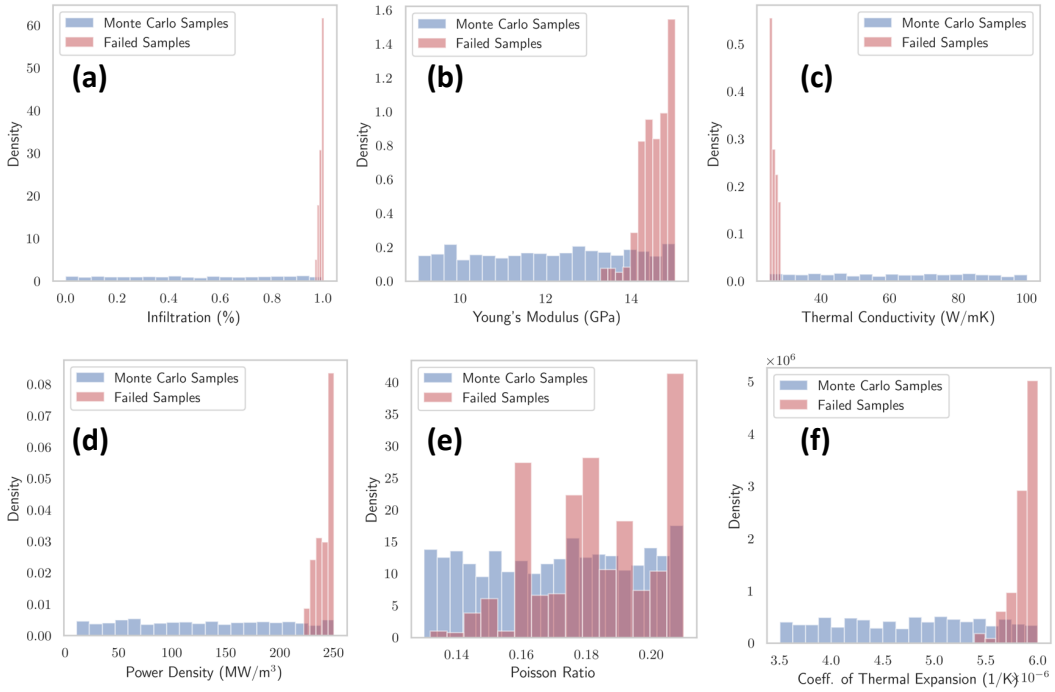

Figure 9. Comprehensive comparison of Monte Carlo samples versus failed samples across different input parameters for simulations conducted using the unit cell of the actual MSRE geometry.

distributions for some parameters have broadened, while others have become less significant. The three most significant parameters in this set of simulations are the infiltration amount, thermal conductivity, and power density. Table 3 compares the previous study and the current study in regard to the failure distribution ranges, providing a more detailed understanding of the changes. As the size of the unit cell geometry increases, the range of parameters contributing to failure widens. For example, in the original MSRE geometry, a minimum infiltration amount of 97% was required to induce failure, whereas in the scaled geometry, an infiltration amount of 81% was sufficient to induce failure.

Table 3. Input parameters considered, along with their respective ranges, from failed samples for original and scaled geometries.

No.	**Variable**	**Original Geometry**		**Scaled Geometry**	
		Min	**Max**	**Min**	**Max**
1	Infiltration Depth	0.97	1	0.81	1
2	Young's Modulus	13.25	15	9.33	15
3	Thermal Conductivity	25	28.27	25	50.41
4	Power Density	221.73	250	145.73	250
5	Poisson's Ratio	0.13	0.21	0.13	0.21
6	Interface Temperature	823	1017	825	1022
7	Heat Transfer Coefficient	3512.76	5473.67	3500.44	5489.29
8	CTE	5.39×10^{-6}	6.00×10^{-6}	3.54×10^{-6}	6.00×10^{-6}

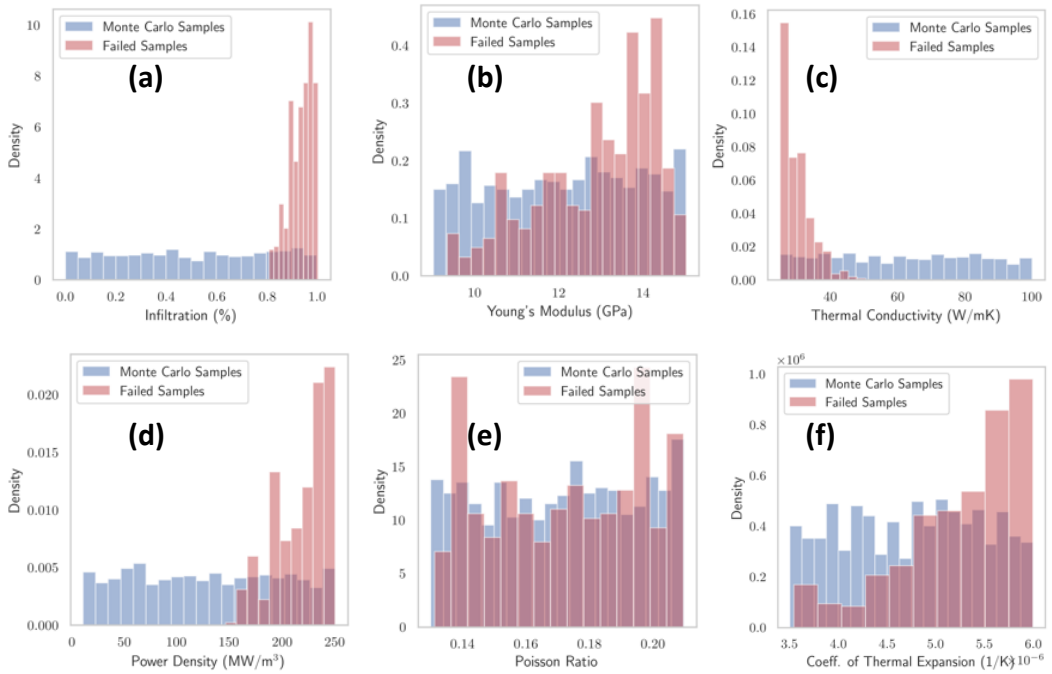

Figure 10. Comprehensive comparison of Monte Carlo samples versus failed samples across different input parameters for simulations conducted using the unit cell of a 150% scaled MSRE geometry.

2.3.4. Hotspot Analysis

In the previous analysis, the effect of pores was accounted for in a homogenized manner by scaling the power density. In the present study, we evaluated the critical size of the pore that could lead to high stress values. These simulations were conducted using the original MSRE geometry. We assumed that the infiltration levels were 100%, and that a single pore existed in the 2D MSRE geometry, shown in Figure 11 as the red colored region. Within this pore, the original value of the power density was applied. It is important to note that the power densities for the other regions were applied in a distributed manner, scaled by the porosity fraction.

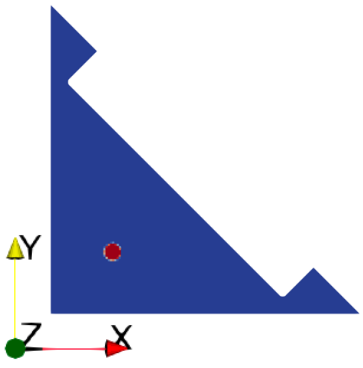

Figure 11. Schematic of the hotspot (represented by the red-colored region) in the 2D MSRE geometry.

Rare-event simulations were conducted for the hotspot analysis by varying the hotspot (or pore) diameter from 0 to 10 mm. Additionally, parameters 2–8, as listed in Table 3, were varied within the same ranges

specified in the table. The distributions of the critical parameters are presented in Figure 12. The region of failure corresponds to a hotspot diameter of greater than 1.4 mm, a thermal conductivity of less than 45 W/mK, and a power density of greater than 143 W/m^3.

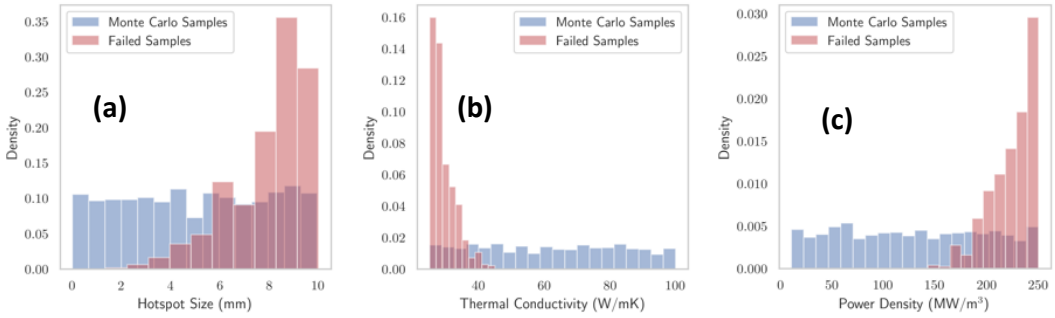

Figure 12. Comprehensive comparison of Monte Carlo samples versus failed samples across different input parameters for simulations conducted using the unit cell of the actual MSRE geometry with a hotspot.

2.3.5. Combined Effects – Infiltration and Radiation

In the previous sections, the simulations focused solely on the effect of molten salt infiltration so as to understand its impact on structural integrity. However, in a reactor environment, a graphite component will be subjected to various effects such as neutron radiation, in addition to the conditions considered in the above sections. This section aims to provide the simulation workflow and inputs to perform a comprehensive analysis for molten salt infiltrated graphite, which is irradiated. Since this requires multi-modal input data dependent on the reactor design, the MSRE geometry and corresponding inputs were chosen. The finite element framework remains the same as detailed in Section 2. The total strain formulation includes additional terms and is given as follows:

$$\epsilon^{total} = \epsilon^{elastic} + \epsilon^{thermal} + \epsilon^{IIDC} + \epsilon^{creep} \tag{4}$$

In this study, we accounted for radiation effects by including two additional strain terms: the irradiation-induced dimensional change (ϵ^{IIDC}) and irradiation creep (ϵ^{creep}). We utilized the Grizzly code's empirical models for ϵ^{IIDC} and ϵ^{creep} [5][g]. Since these models are fitted with experimental data in the pre-turnaround range (neutron fluence of less than 7.5 dpa or $\sim$1e26 n/m^2), and this study primarily focuses on pre-turnaround behavior. The irradiation effects on the material properties were not considered in this study. The objective was to compare the stresses induced by irradiation effects to those caused by molten salt infiltration. For both cases, the material properties remained consistent. Existing Grizzly models do account for material property variations due to radiation. Additionally, if data were uncertain, a PSS framework can be used.

To evaluate the radiation effects, a key input is the neutron flux distribution in the fast spectrum. Steady-state neutron flux data generated using the neutronics simulations performed by Idaho National Laboratory's Griffin team were used as input to this analysis. The axial distribution of the neutron flux, taken at the coolant channel surface, is shown in Figure 13(a), while the radial flux distribution at the center section is shown in Figure 13(b).

Other inputs such as the material properties of graphite, the component geometry, the temperature, and the power density profiles are consistent with those detailed in Section 2. Symmetry boundary conditions

[g]In Grizzly, neutron fluence (defined as flux * time) is provided as input, and the quantities ϵ^{IIDC} and ϵ^{creep} depend on fluence.

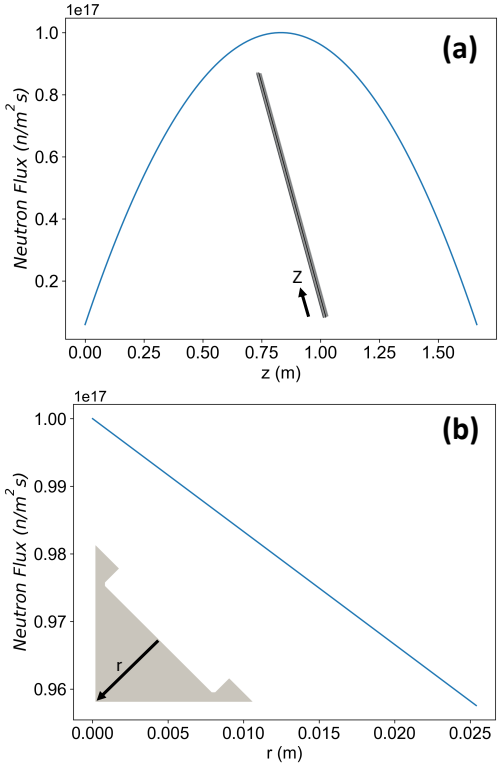

Figure 13. Neutron flux distribution for the MSRE graphite moderator element: (a) in the axial direction along the centerline of the coolant surface channel; (b) in the radial direction at the central section.

were applied to the two faces, as shown in Figure 1(c), while the bottom face had a single point constrained in the axial direction to accommodate deformation due to radiation effects. It is important to note the neutron flux distribution and power density are interrelated and cannot be varied independently, as these parameters are inherently dependent on the specific reactor design under consideration.

Two simulation cases were considered in this study. In the first, we analyzed the stress due to radiation and temperature effects—ignoring infiltration—in order to establish a baseline understanding of the component. In the second case, we considered infiltration effects in addition to radiation, assuming 100% infiltration.

Figure 14 illustrates the distribution of the maximum principal stress due to radiation effects, without any infiltration, at the 60-year mark. This stress distribution significantly differs from that observed in the infiltration-only simulations (Figure 5). In the radiation case, high stresses are concentrated at the ends of the moderator element, whereas in the infiltration-only case, they are centered in the moderator element. The maximum stress observed at the indicated location is approximately 1.4464 MPa.

Figure 15 shows the evolution of the stress value over a period of 60 years at the location of maximum stress (Figure 14) for both radiation only (no infiltration) and radiation with 100% infiltration. When infiltration effects are added to the baseline, the stresses increase marginally to about 1.4558 MPa, representing an approximately 0.65% increase relative to the baseline. This minimal increase in stress is due to the minimal impact of infiltration at the indicated location. Overall, the radiation-induced stresses are notably higher than the infiltration-induced stresses for the baseline MSRE moderator element.

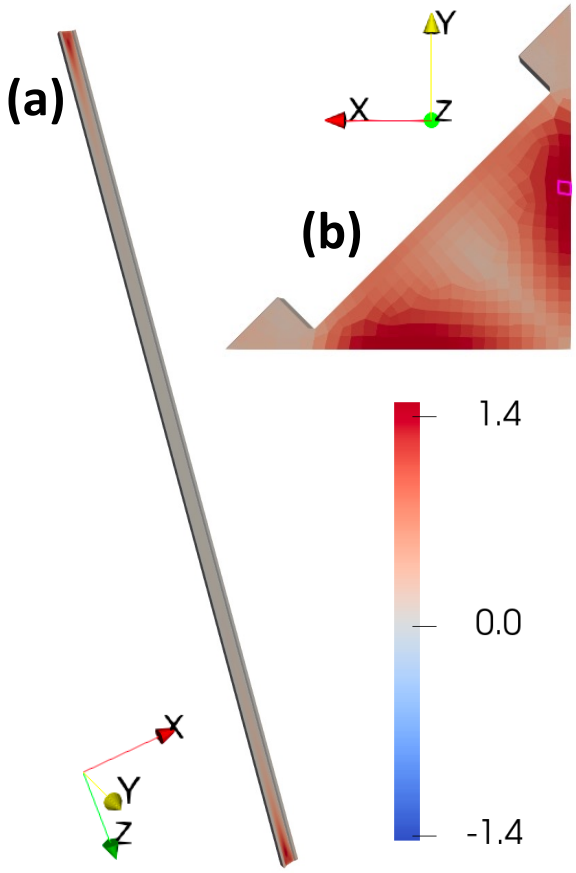

Figure 14. (a) Distribution of maximum principal stress (MPa) on the MSRE graphite moderator element, due to radiation effects, and (b) maximum stress location, as indicated by the pink box on the negative z face.

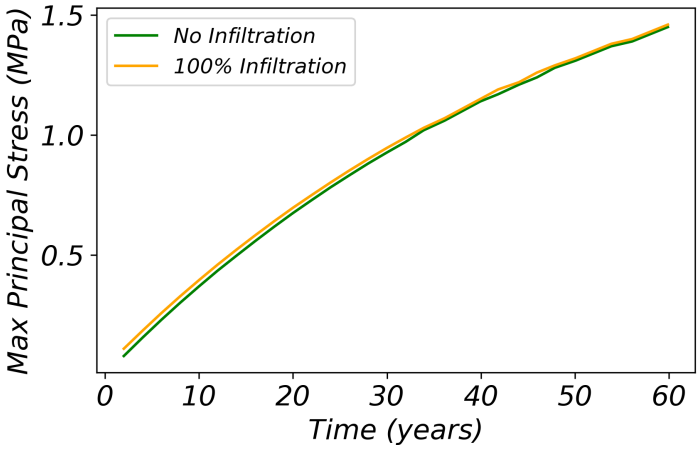

Figure 15. Evolution of the maximum stress value over a period of 60 years at the location of maximum stress (Figure 14) for (a) radiation only (no infiltration) and (b) radiation with 100% infiltration.

2.4. Discussion

The objective of this model was to quantify the role of molten salt infiltration on the structural integrity of graphite in MSR designs. Different graphite grades vary in terms of their susceptibility to infiltration, with ultra-fine and micro-fine graphite grades being the least susceptible. Irradiation results in pore shrinkage, thus affecting the amount of infiltration. Due to lack of data on infiltration levels, we adopted an inverse approach and evaluated conservative infiltration scenarios. Although radiation alters the material properties, we captured this variability by using a PSS framework. Furthermore, steady-state temperature distributions were considered, and transient effects were not included.

The results of this study provide important insights into the structural integrity of graphite components in MSRs. Increasing levels of molten salt infiltration lead to higher induced stresses, but these stresses become critical only under specific conditions involving high infiltration percentages, power densities, and low thermal conductivities. For the MSRE design, the failure probability was calculated to be extremely low at 6.79E-7, based on a failure criterion of 15 MPa. This indicates the likelihood of the graphite moderator reaching critical stress levels is very low for the MSRE design. However, for the scaled geometry, the failure probability was significantly higher at 3.81E-3. The use of ultra-fine and micro-fine graphite grades can significantly reduce the percentage of infiltration.

To analyze the structural integrity of graphite for new grades or MSR designs, a potential approach is as follows. First, the properties of the specific graphite grade (as in Table 1), including temperature and radiation dependencies if available, should be obtained. If unavailable, material testing should be conducted to obtain them. Furthermore, uncertainty analysis is beneficial for those properties that are readily available to account for variations. Next, reactor-specific inputs such as power density and salt temperature at the interface should be obtained. For such inputs, it is beneficial to fit a cosine function for temperature and a polynomial function for power density so as to streamline the modeling process. Afterward, a unit cell model of the graphite moderator should be created, and the diffusion-based problem should be solved to develop a library of pre-computed solutions for infiltration profiles. If accurate information on the percent infiltration for the graphite grade under reactor conditions is available, 3D analysis of the unit cell should be performed to obtain the stress distributions, followed by an ASME full assessment to obtain the failure probability [8].

If several pieces of information are missing, conducting rare-event simulations is a potential path forward (as in Subsection 2.3.3). Preliminary results can be obtained using a 2D generalized plane strain model, as demonstrated earlier; otherwise, full 3D simulations can be conducted for more detailed analysis. This approach enables assessment of new reactor designs and graphite grades, ensuring robust structural integrity evaluations.

Previous paragraphs discussed simulation cases without explicitly accounting for radiation-induced stress effects. Consideration of radiation effects presents significant challenges, requiring additional inputs such as the neutron flux distribution and radiation-dependent parameters, including empirical models for dimensional change and creep specific to the graphite grade in question. In Grizzly, radiation-dependent parameters, including empirical models for dimensional change and creep, are available for three grades of graphite: H451, NBG-18, and IG-110. Obtaining accurate neutron flux distributions for new reactor designs can be particularly difficult. But despite these challenges, if all the necessary data are available, the model may effectively simulate the stresses induced by the combined effects of molten salt infiltration and radiation exposure.

3. ROLE OF WEAR

3.1. Phenomena and Potential Effects

Wear of graphite components used in MSRs can occur due to abrasion and erosion mechanisms. In the pebble-bed MSR design, graphite fuel pebbles can rub against each other and against reactor structures, due to coolant circulation and pebble cycling—potentially resulting in material loss and surface defects. Wear might also occur due to the circulation of dust/particulates carried in by molten salt from other areas of the reactor.

The severity of wear is influenced by various factors such as temperature, environment, and the presence of lubricants. For instance, tribological studies have shown wear and friction to be more pronounced at lower temperatures and in dry conditions. Conversely, higher temperature environments with molten salt (e.g., FLiBe) significantly reduce friction and wear rates, highlighting the protective role of the salt. A detailed review can be found in [4].

The impact of wear extends beyond material loss, as it can introduce surface defects that act as stress concentrators, potentially leading to structural failure. These defects, which form over the course of the component's lifetime, can compromise the integrity and performance of graphite components in MSRs. For this study, we designed simulation cases based on worst-case scenarios, and evaluated the structural integrity of a graphite component.

3.2. Modeling Framework

Using a coupled multiphysics approach, this study aimed to predict the stress induced by the surface wear potentially caused by the sliding and rolling of pebbles on a graphite component. The finite element framework is identical to the one detailed in Section 2.3.5.

In this study, we assumed that wear or a surface defect already existed on the surface of the graphite component. The simulations focused on evaluating the structural integrity of graphite with varying sizes and configurations of surface defects.

3.2.1. Geometry and Inputs

For this study, a pebble bed gFHR design was selected because essential data for the simulations were available in the public domain. The gFHR is a fluoride salt-cooled reactor that uses tri-structural isotropic (TRISO) fuel and relies on graphite as a reflector. IG-110 was chosen for the analysis. As already mentioned, the workflows developed herein may be applicable to any MSR design and graphite grade; however, in this study, the aforementioned specifications were specifically considered.

Two critical inputs for the model were the neutron flux distribution and the temperature distribution of the reflector component. Relevant data were obtained from the neutronics simulations performed at Idaho National Laboratory [9]. These data were then fitted with appropriate functions to facilitate implementation. Figures 17(a) and (b) show the neutron flux distributions and their corresponding fits. Figure 17(a) presents the neutron flux along the axial direction at the inner surface (r = 1.2 m), and Figure 17(b) displays the neutron flux variation along the radial direction at the point of maximum axial flux.

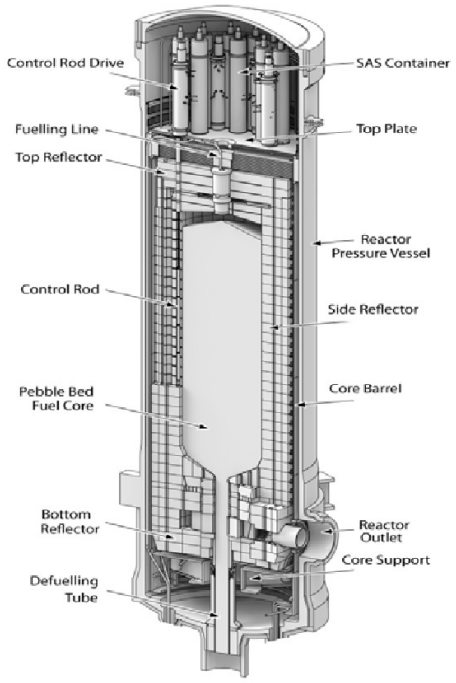

Figure 16. Cross-section view of a pebble-bed reactor, showing the modular blocks of the reflector. (Image reproduced from [2][h].)

The functional forms for the neutron flux distribution thus obtained are as follows:

$$F^{\max}(z)\big|_{r=1.2\,\mathrm{m}} = 1.26\times10^{15}\cdot z^3 - 1.26\times10^{16}\cdot z^2 + 3.20\times10^{16}\cdot z - 1.89\times10^{15} \tag{5}$$

$$F(x,y,z) = F^{\max}(z)\big|_{r=1.2\,\mathrm{m}} \cdot \exp\left(-11.77\cdot\left(\sqrt{x^2+y^2}-1.26\right)\right) \tag{6}$$

Figures 17(c) and (d) present the temperature distribution along the axial direction at the inner and outer surface, respectively, and the functional forms are as follows:

$$T\big|_{r=1.2\,\mathrm{m}} = -36.41\cdot\cos(z-0.58) + 899.49 \tag{7}$$

$$T\big|_{r=1.8\,\mathrm{m}} = -30.74\cdot\cos(z-0.59) + 899.85 \tag{8}$$

$$T(x,y,z) = T\big|_{r=1.2\,\mathrm{m}} - \left(\frac{T\big|_{r=1.2\,\mathrm{m}} - T\big|_{r=1.8\,\mathrm{m}}}{0.6}\right)\cdot\left(\sqrt{x^2+y^2}-1.2\right) \tag{9}$$

[h]Note that this is not a fluoride salt reactor. The reason for showing this figure is to illustrate the arrangement of the modular graphite blocks and to emphasize that it is not a single monolithic block.

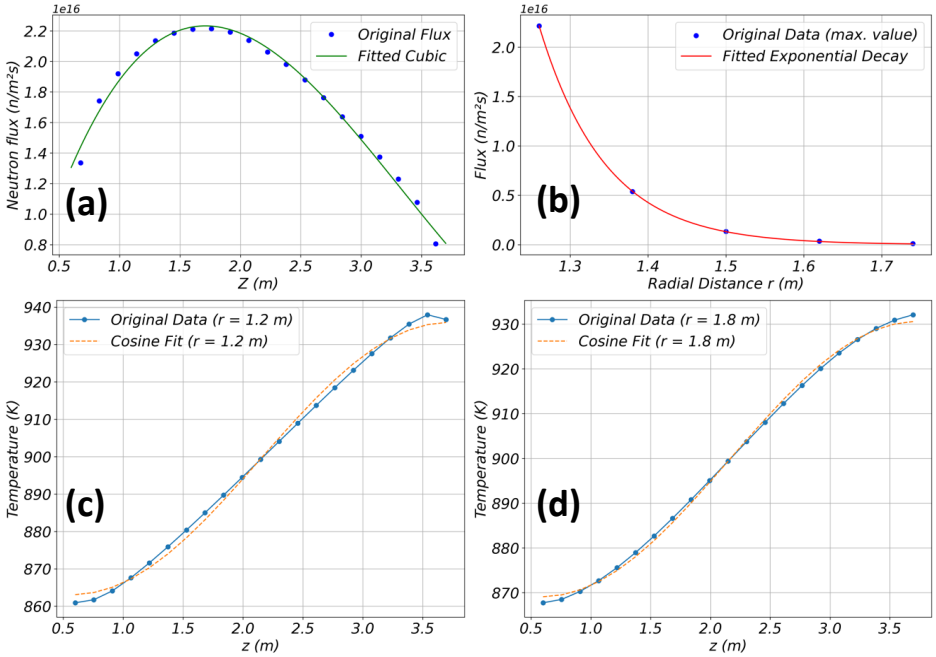

Figure 17. (a) Neutron flux distribution at the inner surface (r = 1.2 m) along the axial direction. (b) Neutron flux distribution along the radial direction at the axial maximum. Also shown is the temperature distribution along the axial direction at the (c) inner surface (r = 1.2 m) and (d) outer surface (r = 1.8 m).

3.2.2. Finite Element Model

The graphite reflector is an assembly of many modular blocks, as shown in Figure 16. For the present study, we focused primarily on those blocks that formed the inner surface of the reflector, as this is where the pebbles slide over them. These blocks were assembled via interlocking mechanisms such as keys or dowels [10]. A schematic of an individual reflector block is shown in Figure 18.

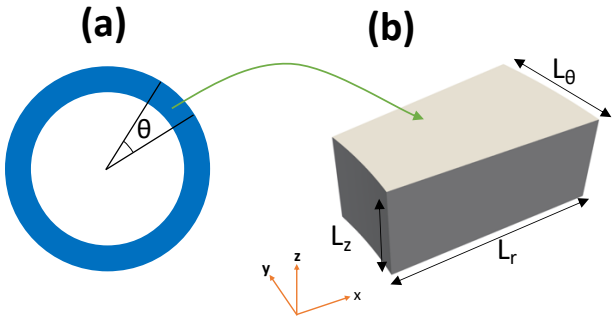

Figure 18. (a) Top section view of the side reflector. (b) Schematic of a single reflector block with geometrical parameters.

As this study primarily focused on the pre-turnaround stage, where graphite experiences bulk volume shrinkage, it was reasonable to assume that no individual block had any substantial force transfer or interactions. Therefore, only a single block was investigated through the finite element simulation. The block geometry was meshed with 3D hexahedral elements. The following constraints were applied at three points in the block to prevent any rigid body motion. All three points are present on the visible r-z plane in Figure 18(b). The

first point is on the lower left of the plane and is constrained in all three translations. The second point is at the top left and has a constraint in y. The last point is at the bottom right and is constrained in y and z.

3.2.3. Simulation Strategy

The precise number of blocks constituting the reflector component for the fluoride high-temperature reactor design was not publicly available. Therefore, an alternative methodology was employed. Based on the maximum dimensions of the graphite block, as specified by the manufacturer's data, we evaluated several geometries to identify worst-case scenarios interms of maximum stress induced. For an isopressed graphite available in the public domain, the graphite blocks measure 305 mm x 610 mm x 1550 mm[i]. Preliminary simulations indicated that induced stress rises with increasing block size. Consequently, a total of eight cases were designed to maximize the dimensions while still adhering to the manufacturing block size constraints, including a few cases aimed at understanding sensitivity. Table 4 presents the geometrical parameters using various length descriptors, as illustrated in (Figure 18[b]).

Table 4. Geometrical parameters for different simulation cases.

Case #	θ (degrees)	L_r (m)	L_z (m)	L_θ (m)
1	9.72	0.6	1.55	0.305
2	51	0.6	0.305	1.550
3	19.5	0.3	1.55	0.610
4	51	0.3	0.61	1.550
5	30	0.6	0.305	0.932
6	9.72	0.6	0.8	0.305
7	25	0.6	0.305	0.779
8	51	0.3	0.305	1.550

The cases presented above are baseline simulation scenarios that do not account for any wear defects. Following completion of the simulations and analysis, the geometry that induces the maximum principal stress will be selected for further examination. Specifically, a surface defect will be modeled on the inner surface of the block, and the sizes of these defects will be varied to assess their impact on the induced stress. Additionally, based on the critical defect size, the wear rate will be estimated and compared to existing wear rates obtained from experiments in order to determine the plausibility of this scenario.

Realistic surface wear profiles are inherently complex, and obtaining such data from the public domain can be challenging. In this study, we idealized these defects as pits and grooves, as illustrated in Figure 19. By varying the sizes of these grooves and pits, we aimed to understand their impact on the induced stress.

[i]Note that the data provided for the ET-10 graphite grade from the IBIDEN datasheet is not directly applicable to the IG-110 block used in the simulations. However, it has been used as an approximate value for the purposes of this analysis.

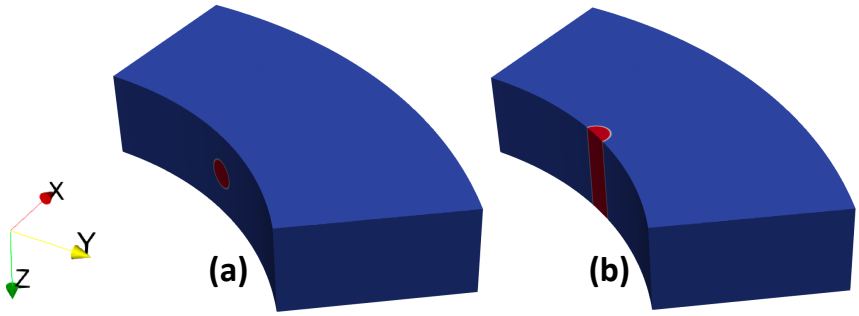

Figure 19. Schematic of a (a) pit and a (b) groove type surface wear defect.

3.3. Results

Finite element simulations were conducted on the eight identified cases, and Table 5 presents the maximum principal stresses near the inner surface, as well as the maximum stresses for the entire block. It is observed that the maximum stress of the entire block exceeds the stresses induced at the inner surface. This is likely due to the gradient in the neutron flux distribution, which is higher at the inner surface and much lower at the outer surface. Consequently, the inner surface undergoes more deformation than the outer one. This gradient in deformation could explain the high stresses observed at the edges. However, for this study, which focuses on the effect of wear, the stresses near the inner surface are more critical.

The maximum stresses near the surface occur in case 2, which has the largest dimension in the azimuthal direction. Comparison of cases 2 and 5 reveals that adding more material induces increased stress. A similar observation can be made from cases 1 and 6. This is likely because adding more material introduces greater geometrical constraints to the deformation, resulting in increased stresses.

Figure 20 shows the evolution of maximum stresses near the inner surface over time, for up to 60 years. The general trend indicates that the stresses initially increase, but then decrease after reaching a peak. This behavior is primarily driven by the evolution of different components of strain over time, as described by Equation 4. We assumed a steady-state temperature distribution, meaning that the thermal strains remained constant. However, the strains due to IIDC and creep evolve over time. According to Equation 4, the elastic strain also changes, affecting the stresses. As time progresses, the creep strain increases, thus relaxing the stress by reducing the elastic strain.

Figure 21 shows the distribution of maximum principal stress for case 2. It is observed that the stresses are highest at the edges of the block, and that the stress near the surface is lower than the overall maximum.

It is important to note that the cases discussed above represent worst-case scenarios. However, a single simulation was also performed using more realistic geometric parameters: $\theta = 12^{\circ}$, $L_r = 0.6$ m, and $L_z = 0.25$ m. In this scenario, the maximum stresses near the inner surface were found to be 3.7 MPa.

From the results above (Table 5), case 2 was chosen for analyzing the effects of wear. More specifically, we aimed to understand the extent to which wear defects would increase the stresses beyond the baseline results due to stress concentration.

To that end, the role of wear was analyzed by setting up (1) two cases with a pit configuration and (2) two cases with a groove configuration. As shown in Figures 22(b)–(d), the configurations had two distinct radii (i.e., 0.01 and 0.05 m, as compared to the annular width of 0.6 m). Figure 22(a) shows the distribution of the maximum principal stress on a slice of the block, normal to the z-plane. It illustrates that the stresses are higher near the inner surface but rapidly decrease as we move away in the radial direction.

Table 5. Maximum stress values for different simulation cases.

Case #	Max. stress near the inner surface (MPa)	Max. stress for the whole block (MPa)
1	9.88	14.48
2	11.12	17.28
3	8.33	13.53
4	8.58	14.26
5	10.21	17.17
6	9.21	14.68
7	9.39	16.84
8	7.20	10.84

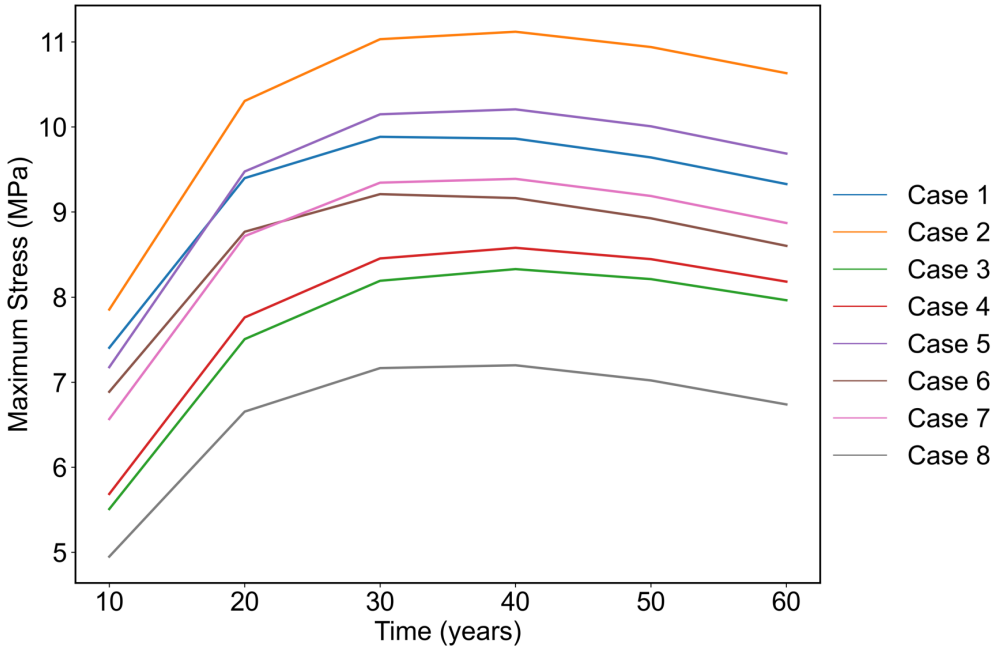

Figure 20. Temporal evolution of maximum stress values for baseline scenarios without wear, observed near the inner surface.

From Figures 22(b)–(d), we see that the groove configurations are more detrimental than the pit cases. The maximum stress observed for a groove radius of 0.05 m was 18 MPa, representing a 62% increase over the baseline cases.

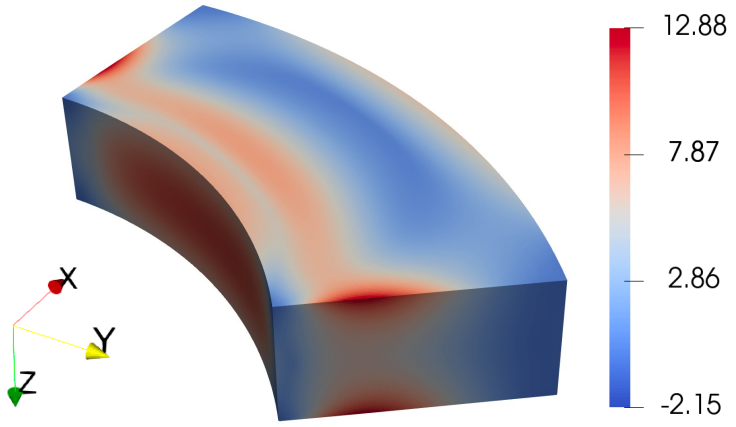

Figure 21. Distribution of maximum principal stress (MPa) for case 2 at 40 years, corresponding to the maximum stress value.

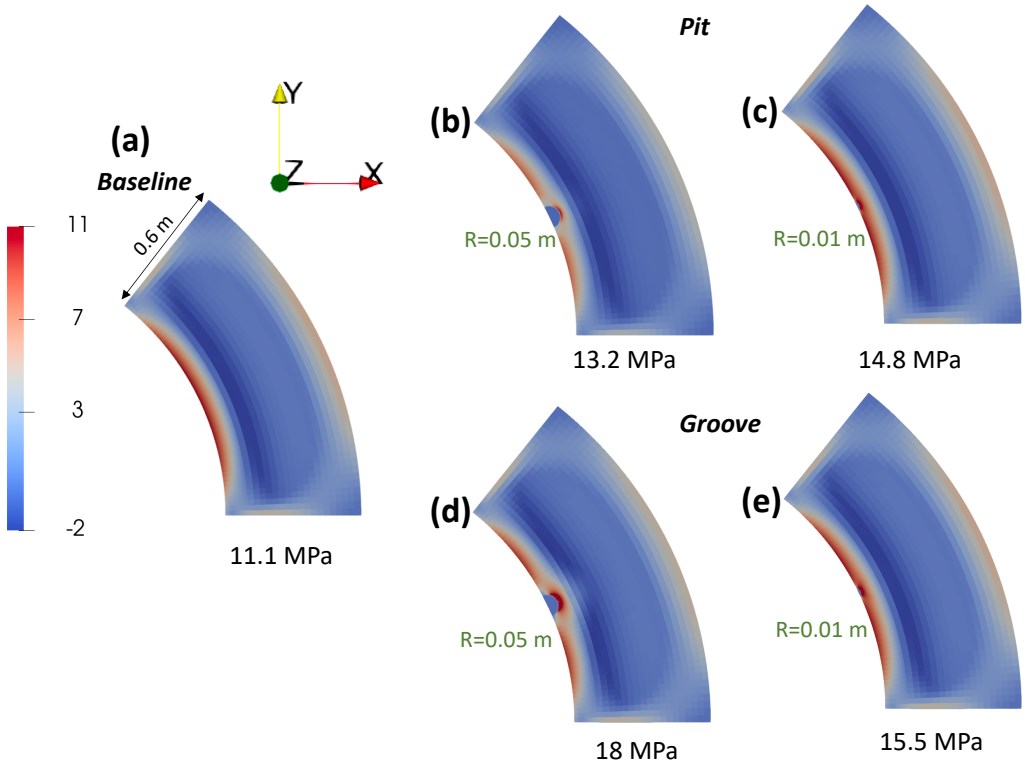

Figure 22. Distribution of maximum principal stress (MPa) at 40 years for (a) the baseline case (case 2) at a cross section corresponding to the maximum stress value, (b) baseline case with a pit of radius 0.05 m, (c) baseline case with a pit of radius 0.01 m, (d) baseline case with a groove of radius 0.05 m, and (e) baseline case with a groove of radius 0.01 m.

3.4. Discussion

In the previous section, we set up simulations to predict the stresses caused by pits and grooves under worst-case scenarios. It is evident that pit formation would occur much faster than groove formation, given the smaller volume of material to be removed. By assuming that a pit with a radius of 0.01 m forms over 60 years, we back-calculated the wear rate required to create such a pit. To evaluate the feasibility of this scenario in a real reactor, we compared the calculated wear rate against experimental wear rates measured in laboratory settings. This comparison helps us determine the likelihood of forming a pit with a radius of 0.01 m over a 60-year period.

The following is an approximate calculation of wear rate for creating a pit of radius 0.01 m, assuming that the pebbles are continuously sliding on the surface of the reflector block.

Wear diameter: 0.02 m

Average velocity of pebble: $3.5 - 15$ cm/day [9, 11]

In the calculation below, a velocity of 15 cm/day was considered in order to determine the worst case scenario.

Number of passes per day:

$$\text{Number of passes per day} = \frac{\text{velocity}}{\text{diameter}} \approx 7.5$$

Sliding distance for 60 years:

$$\text{Sliding distance for 60 years} \approx 7.5 \times 0.02 \times 21915 \approx 3300\,\text{m}$$

Wear volume:

$$\text{Wear volume} = \frac{2}{3}\pi R^3 \approx 2.1 \times 10^{-6}\,\text{m}^3$$

The maximum normal force between the pebble and the reflector block was taken to be $\sim$100 N [11].

Wear rate:

$$\text{Wear rate} = \frac{\text{Wear volume}}{\text{distance} \times \text{load}} \approx 6.36 \times 10^{-12}\,\text{m}^3/\text{N-m} \approx 6.36 \times 10^{-3}\,\text{mm}^3/\text{N-m}$$

The worst-case scenario wear rate of $6.36 \times 10^{-3}\text{mm}^3/\text{N-m}$ is at least 13 times higher than the wear rate of $4.7 \times 10^{-4}\text{mm}^3/\text{N-m}$ observed in wear experiments conducted under a dry argon environment [11]. This means that, under reactor conditions, a pit with a radius of 0.01 m is unlikely to form within the 60-year lifespan intended for this design. Consequently, other cases of pits and grooves are also unlikely to develop. The present analysis was based on the least critical scenario among the four cases shown in Figure 22 and considered a worst-case reflector block. Under more realistic conditions, including lubrication and a reflector block with practical dimensions, the induced stress is expected to be significantly lower. It is noted that the experimental wear rate was assumed to occur under steady-state conditions—an assumption that may be inaccurate. Long-term experiments evaluating the steady-state wear rate would be beneficial in improving the accuracy of this type of analysis. This study assumes that irradiation does not impact the wear rate; however, this effect may need to be evaluated in a more detailed analysis.

To evaluate wear in new MSR designs or graphite grades, a potential approach is as follows. First, the properties of the specific graphite grade, including any available temperature and radiation dependencies,

should be obtained. Reactor-specific inputs such as reflector block geometry and neutron flux distribution are essential. Obtaining the neutron flux distribution presents a moderate challenge, as it requires running neutronics simulations to determine the neutron flux in the fast spectrum. Furthermore, model parameters for capturing irradiation-induced dimensional change and irradiation creep are important for the graphite grade under consideration. Obtaining these model parameters may present the most significant challenge, as it involves years of dedicated experiments under different temperatures and dosages. Alternatively, a mechanistic model[j] could help, but such models are currently unavailable in the literature.

Despite these challenges, if all the necessary data stated above are available, the model may effectively simulate the stresses induced by the combined effects of wear, neutron flux, and radiation exposure. This approach ensures that the structural integrity of graphite components in new reactor designs and graphite grades can be thoroughly assessed, accounting for the complex interplay between wear and radiation effects.

4. CONCLUSIONS

Nuclear graphite is being considered for use in many molten salt reactor designs due to its favorable structural and neutronic properties However, graphite can potentially degrade when exposed to molten salt environments, and currently, the impact of these degradation mechanisms on structural integrity of graphite is not thoroughly understood. In this report, finite element modeling and simulation was employed to quantitatively evaluate two critical graphite degradation mechanisms in MSRs: molten salt infiltration into graphite moderator elements in fuel-salt designs and surface wear of graphite reflectors in pebble-bed reactor designs. The analysis was structured to systematically assess the structural integrity of graphite under these mechanisms.

The first part of this study focused on the structural impact of molten salt infiltration, particularly examining the stresses caused by internal heat generation from fission process arising from infiltrated fuel salt. A representative moderator geometry from the MSRE design was modeled and the stress analysis was conducted. Results indicated that even with a 100% infiltration, the stresses ($\sim$0.13 MPa) remained significantly below the allowable limits of the graphite grade considered in the analysis. To account for uncertainties, additional analyses using parallel subset simulation (PSS) were performed. Key parameters such as graphite moderator geometry, thermal conductivity, power density, infiltration depth were systematically varied to assess their influence on structural integrity. PSS analysis on the baseline MSRE geometry revealed a very low failure probability of failure ($\sim$ 1 in 1.5 million). However, a geometry uniformly scaled by 150% exhibited a significantly higher probability of failure ($\sim$ 1 in 262). To assess the impact of larger pores due to manufacturing variance, PSS analysis were conducted. PSS analysis indicated that pores larger than 1.4 mm could potentially cause structural concerns. Additionally, simulations combining irradiation effects with infiltration revealed that irradiation-induced stresses were notably higher than infiltration-induced stresses for the baseline MSRE moderator.

The second part of this study focused on evaluating the role of surface wear on the structural integrity of graphite blocks in pebble-bed reactor designs. Due to non-availability of relevant data, worst-case scenarios were developed and analyzed. Finite element simulations were conducted on multiple block geometries to identify the geometry that exhibits the highest stress due to combined irradiation and thermal effects, in the absence of wear. The block with the largest dimension in the azimuthal direction had the maximum stresses near the inner surface of the block. This geometry was selected to investigate the effect of idealized pre-existing

[j]A multi-scale model would be appropriate. Lower-length-scale simulations using molecular dynamics and cluster dynamics can provide information on the quantification of defect generation and evolution. A crystal plasticity model incorporating this lower-length-scale information and macroscale heterogeneities could provide the radiation- and temperature-dependent bulk response.

defects in the form of pits and groove configurations. Pits and grooves with different sizes were investigated to understand the stress concentration induced by them over a long-term operation of the reactor. The presence of a groove with 0.05 m radius led to an increase of the maximum principal stress by approximately 62% compared to the no-defect baseline case. Pit shaped defects had a lesser impact as compared to the groove configurations. To evaluate the likelihood of such damage developing in-service, wear rates required to from these defect sizes over a 60 year operational period were estimated. The preliminary analysis showed that the required wear rate ($\sim$6.36e-3 $mm^3/N\text{-}m$) to form a 0.01 m pit type defect exceeded current experimental observed rate ($\sim$4.74e-4 $mm^3/N\text{-}m$) by more than an order of magnitude, suggesting such extreme surface degradation is unlikely under operating condition, under the assumptions considered in the analysis.

Overall, this study provided advanced modeling and simulation strategies for assessing the performance of graphite components in MSRs. The simulation approaches, including the coupled multiphysics framework and rare-event simulation techniques, offer a robust foundation for evaluating structural integrity, considering various effects such as thermal loading, infiltration, radiation, and wear. These tools are adaptable to various geometries and graphite grades, and support future investigations aimed at optimizing material selection, component design, and long-term reactor safety.

5. REFERENCES

[1] https://mooseframework.inl.gov/source/samplers/ParallelSubsetSimulation.html.

[2] W. Windes, G. Strydom, R. Smith, and J. Kane, "Role of nuclear grade graphite in controlling oxidation in modular HTGRs," Tech. Rep. INL/EXT-14-31720, Idaho National Laboratory, 2014.

[3] M. Srinivasan, B. Marsden, W. von Lensa, L. Cronise, and R. Turk, "Appendices to the assessment of graphite properties and degradation, including source dependence," Tech. Rep. TLR/RES/DE/REB-2021-08, U.S. Nuclear Regulatory Commission, August 2021.

[4] V. Prithivirajan, "Examining Graphite Degradation in Molten Salt Environments: A Chemical, Physical, and Material Analysis," Tech. Rep. TLR-RES/DE/REB-2024-14, INL/RPT-23-75892, Idaho National Laboratory (INL), Idaho Falls, ID (United States), 08 2024.

[5] P. Bajpai, V. Prithivirajan, L. B. Munday, G. Singh, and B. W. Spencer, "Development of Graphite Thermal and Mechanical Modeling Capabilities in Grizzly," Tech. Rep. INL/RPT-24-78905, Idaho National Laboratory (INL), Idaho Falls, ID (United States), 05 2024.

[6] R. C. Robertson, "MSRE Design and Operations Report, Part I: Description of Reactor Design," Tech. Rep. ORNL-TM-0728, Oak Ridge National Laboratory, Oak Ridge, TN, January 1965.

[7] M. K. Mohammad Jaradat and J. Ortensi, "Thermal spectrum molten salt-fueled reactor reference plant model," Tech. Rep. INL/RPT-23-72875, Idaho National Laboratory (INL), Idaho Falls, ID (United States), 07 2023.

[8] *Understanding the Semi-Probabilistic Approaches in Structural Reliability Used to Set Design Reliability Targets for Graphite Components Using ASME BPVC Methods*, vol. Volume 1: Codes Standards; Computer Technology Bolted Joints of *Pressure Vessels and Piping Conference*, 07 2024.

[9] J. Ortensi, C. M. Mueller, S. Terlizzi, G. L. Giudicelli, and S. Schunert, "Fluoride-Cooled High-Temperature Pebble-Bed Reactor Reference Plant Model," Tech. Rep. INL/RPT-23-72727, Idaho National Laboratory (INL), Idaho Falls, ID (United States), 05 2023.

[10] M. E. Tano and J. C. Ragusa, "Coupled Computational Fluid Dynamics–Discrete Element Method Study of Bypass Flows in a Pebble Bed Reactor," *Nuclear Technology*, vol. 207, no. 10, pp. 1599–1614, 2021.

[11] T. Grejtak, J. Qu, N. C. Gallego, and J. R. Keiser, "Report on Initial Tribological Studies of Graphite in Dry Argon and Molten Salt Environment," Tech. Rep. ORNL/TM-2024/3253, Oak Ridge National Laboratory (ORNL), Oak Ridge, TN (United States), 01 2024.